Organic Electronics 13 (2012) 796–806

Contents lists available at SciVerse ScienceDirect

Organic Electronics

journal homepage: www.elsevier.com/locate/orgel

High performance organic light emitting diodes using substoichiometric tungsten oxide as efficient hole injection layer

Maria Vasilopoulou [a,*], George Papadimitropoulos [a], Leonidas C. Palilis [b], Dimitra G. Georgiadou [a], Panagiotis Argitis [a], Stella Kennou [c], Ioannis Kostis [a,d], Nikolaos Vourdas [a], Nikolaos A. Stathopoulos [d], Dimitris Davazoglou [a]

[a] Institute of Microelectronics, NCSR Demokritos, Terma Patriarchou Grigoriou, 15310 Aghia Paraskevi, Greece
[b] Department of Physics, University of Patras, 26500 Patras, Greece
[c] Department of Chemical Engineering, University of Patras, 26500 Patras, Greece
[d] Department of Electronics, Technological and Educational Institute of Pireaus, 12244 Aegaleo, Greece

ARTICLE INFO

Article history:
Received 20 September 2011
Received in revised form 11 January 2012
Accepted 15 January 2012
Available online 31 January 2012

Keywords:
Transition metal oxides
Reduced metal oxides
Metallic suboxides
Organic light emitting diodes
Efficient hole injection

ABSTRACT

In this work we demonstrate the unique hole injection and transport properties of a substoichiometric tungsten oxide with precise stoichiometry, in particular $WO_{2.5}$, obtained after the controlled hydrogen reduction during growth of tungsten oxide, using a simple hot-wire vapor deposition technique. We present clear evidence that tungsten suboxide exhibits metallic character and that an almost zero hole injection barrier exists at the anode/polymer interface due to the formation/occupation of electronic gap states near the Fermi level after oxide's reduction. These states greatly facilitate hole injection and charge generation/electron extraction enabling the demonstration of extremely efficient hole only devices. $WO_{2.5}$ films exhibit metallic-like conductivity and, thus, can also enhance charge transport at both anode and cathode interfaces. Electroluminescent devices using $WO_{2.5}$ as both, hole and electron injection layer, and poly[(9,9-dioctylfluorenyl-2,7-diyl)-co-(1,4-benzo-{2,1′,3}-thiadiazole)] (F8BT) as the emissive layer exhibited high efficiencies up to 7 cd/A and 4.5 lm/W, while, stability studies revealed that these devices were extremely stable, since they were operating without encapsulation in air for more than 700 h.

1. Introduction

Organic light-emitting diodes (OLEDs) have generated tremendous research interest driven by the expectation of low cost, light weight and mechanically flexible displays and light sources [1–4]. In order to meet the need for lower power consumption and higher operational stability, it is crucial to enhance carrier injection from both electrodes [5–7]. In recent years, the use of metal oxides as anode and cathode interfacial layers has been continuously increasing, since several groups have demonstrated that they enhance both hole and electron injection, while at the same time stable, encapsulation-free, hybrid organic–inorganic light emitting diodes can be realized [6–14]. Especially, transition metal oxides (TMOs), such as molybdenum (MoO_3), tungsten (WO_3) and vanadium (V_2O_5) oxides, have been established as efficient hole injection layers (HILs) in OLEDs due to their ability to exchange charges with several organic semiconductors [8–10,15–23]. Such metal oxide films play also an important role as charge generation layers in tandem OLEDs [24–26]. Although initially they had been considered as p-type wide bandgap semiconductors, recent reports on the electronic structure of thermally evaporated molybdenum, tungsten and vanadium oxides revealed that they primarily exhibit intrinsic n-type semiconducting properties due to the presence of defect bandgap states attributed to oxygen vacancies present in their lattice [15–17,32,33,37].

* Corresponding author.
E-mail address: mariva@imel.demokritos.gr (M. Vasilopoulou).

1566-1199/$ - see front matter © 2012 Elsevier B.V. All rights reserved.
doi:10.1016/j.orgel.2012.01.008

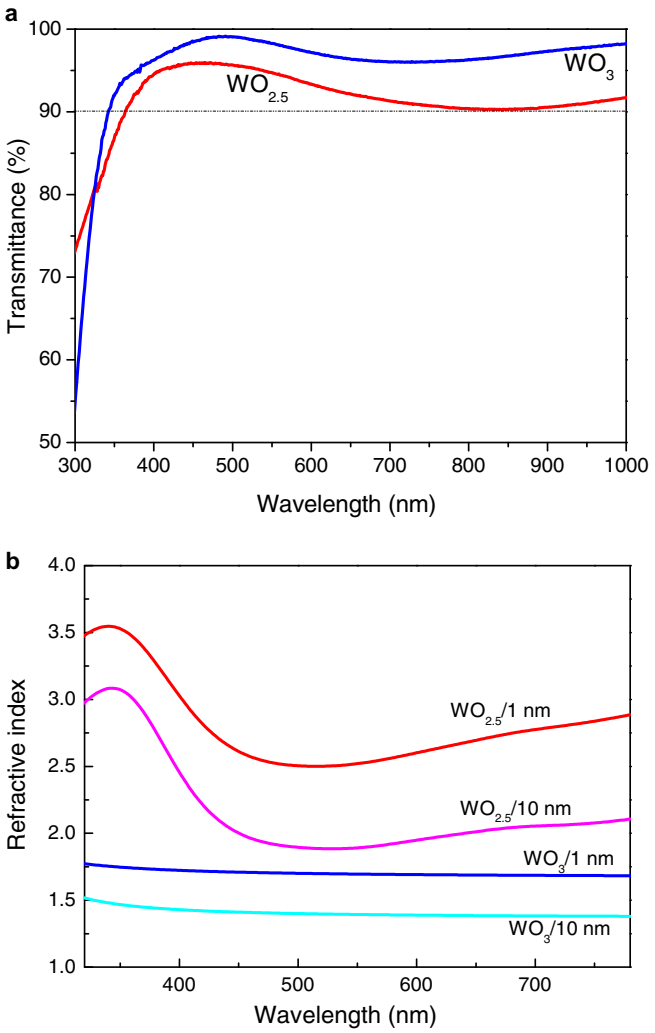

Fig. 1. (a) Transmittance spectra of 10 nm thick films of WO_3 and $WO_{2.5}$. (b) Variation of the refractive index in the optical wavelength region for WO_3 and $WO_{2.5}$ of 1 and 10 nm thickness.

Indeed, when these metal oxides are deposited through metal evaporation, they are usually oxygen deficient and thus, non-stoichiometric, showing defect states and increased electrical conductivity and interesting electronic properties [35–38]. In very recent studies, oxygen deficient substoichiometric MoO_x, NiO_x and CuO_x films have been suggested to serve as effective anode interfacial layers in polymer solar cells [27–30] and OLED devices [31–34]. Despite the fact, that tungsten oxide films exhibit similar properties of those to molybdenum oxides, up to date there aren't any literature results concerning the use of substoichiometric WO_x films as efficient hole injection/extraction layers in organic electronic devices, with the exception of unintentionally reduced tungsten oxide films, due to sputter deposition of ITO overlayer, which have been employed as hole injection and buffer layer in a highly efficient reverse OLED device [16]. These tungsten oxide films exhibit polycrystalline structure and slight coloration, both of which are evidence for the presence of W^{+5} states, since it is widely known that stoichiometric WO_3 is highly transparent and grows amorphously [35].

In our recent publications, hydrogen reduced tungsten and molybdenum oxide films, grown using a simple hot-wire vapor deposition technique, were found to exhibit a large density of occupied sub-bandgap states after reduction [39,40]. The states which were located near the Fermi level were employed for the enhancement of electron injection and transport from the Al Fermi level to the lowest occupied molecular orbital (LUMO) of poly[(9,9-dioctylfluorenyl-2,7-diyl)-co-(1,4-benzo-{2,1′,3}-thiadiazole)] (F8BT). In this work, we extend our previous study to demonstrate the unique hole injection and transport properties of substoichiometric tungsten oxide, in particular $WO_{2.5}$, obtained after the controlled reduction in hydrogen-rich ambient during deposition of tungsten oxide. We also reveal the exact hole injection mechanism in F8BT-based OLEDs incorporating $WO_{2.5}$ as HIL. Finally, relevant results concerning the films' electronic properties, morphology,

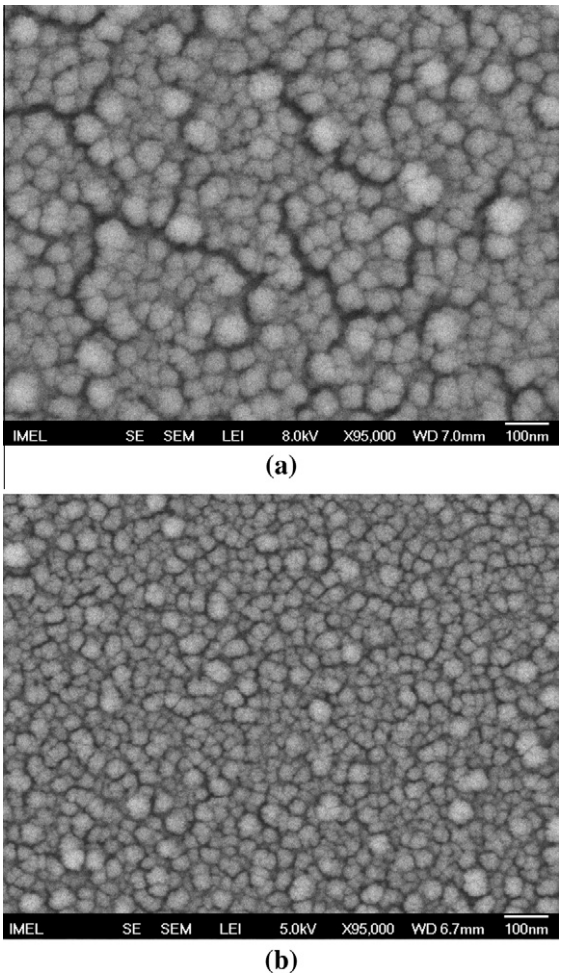

Fig. 2. Scanning electron microscopy images of (a) tungsten trioxide and (b) tungsten suboxide, 30 nm thick films.

composition, optical and electrical properties, as well as their implementation in hole only and electroluminescent devices with high efficiencies and time stability, are presented and discussed.

2. Materials and methods

2.1. Materials

W filament (diameter 0.5 mm) was purchased from Strem. ITO-coated glass substrates (2×2 cm) with a sheet resistance 20 Ω/cm^2 were obtained from Aldrich. Poly(3,4-ethylenedioxythiophene) poly(styrenesulfonate) (PEDOT-PSS) was purchased from Aldrich, while poly[(9,9-dioctyl-fluorenyl-2,7-diyl)-co-(1,4-benzo-{2,1′,3}-thiadiazole)] (F8BT) was purchased from American Dye Source and used as received.

2.2. Tungsten oxide films deposition

Hot-wire tungsten oxide films were deposited by heating a tungsten (W) filament in a vacuum chamber at a filament temperature of 560 °C and at pressure of 5 mTorr. Substrates were placed at a distance of approximately 5 cm from the filament and thus, organic interlayers were kept very close to room temperature during metal oxide films deposition. The films that were deposited in an oxygen environment were fully stoichiometric (WO_3), while films deposited in environment containing 10% H_2 (and 90% N_2) were substoichiometric. Their exact stoichiometry was defined in our previous publication using X-ray photoelectron spectroscopy (XPS) and was found to be W: 1, O: 2.5 (±0.1) [40]. Their stability over a period of months in air exposure was also verified previously [40]. Film thickness was controlled upon varying the deposition time. The deposition rates were 0.5 nm/s for the stoichiometric and 0.25 nm/s for the substoichiometric tungsten oxides. More details on the deposition technique are given elsewhere [41,42].

2.3. Films characterization

The valence band spectra of tungsten oxides were evaluated after recording the Ultraviolet Photoemission (UPS) spectra of 10 nm thick films deposited on ITO substrates taken from the same batch used for OLEDs fabrication. For the UPS measurements the HeI (21.22 eV) excitation line was used. A negative bias of 12.28 V was applied to the sample during UPS measurements in order to separate sample and analyzer high binding energy cut-offs and estimate the absolute work function value from the UPS spectra. The analyzer resolution is determined from the width of the Au Fermi edge to be 0.16 eV. Transmittance and absorption measurements were performed with a Perkin Elmer Lamda 40 UV/Vis spectrophotometer. The film thickness as well as the dispersion of the refractive indices and extinction coefficients were measured using a J.A. Woollam Inc. M2000F rotating compensator ellipsometer (RCE™) running the WVASE32 software at an angle of incidence of 75.14°. Surface morphology was evaluated using Scanning Electron Microscopy (SEM) images taken with a LEO Supra 35 VP instrument. It should be mentioned that oxide layers were exposed to ambient environment in all cases before deposition of the organic semiconductor during device fabrication and, also, before UPS, optical and electrical measurements.

2.4. Fabrication of hole-only and OLED devices

Hole-only devices (HODs) and OLEDs were fabricated on ITO-coated glass serving as the anode. Substrates were ultrasonically cleaned following a standard regime with acetone and isopropanol but without being subject to any oxygen plasma treatment. The tungsten oxide layer was then deposited followed by an approximately 70 nm thick layer of the active, F8BT-based layer, which was spin coated from a chloroform solution (8 mg/ml). After deposition, the device was annealed at 80 °C for 10 min in air. Then, in certain electroluminescent devices, a tungsten suboxide ($WO_{2.5}$) layer about 2 nm thick was deposited on top of the F8BT, to serve as an electron injection/transport layer. The devices were completed by depositing a

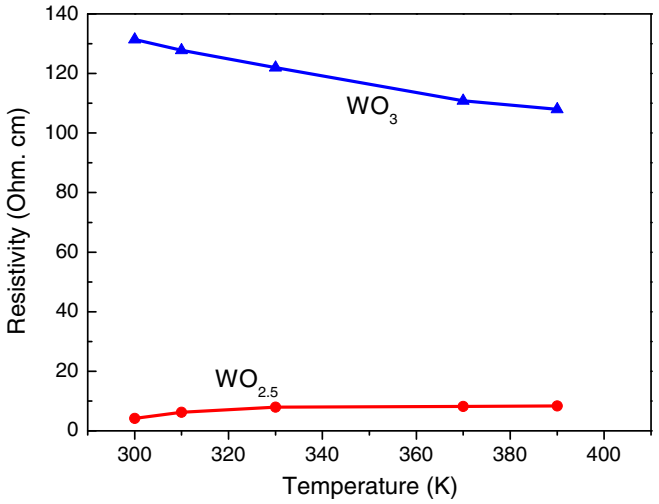

Fig. 3. Resistivity measurements versus temperature for both stoichiometric tungsten oxide and tungsten suboxide, 5 nm thin films.

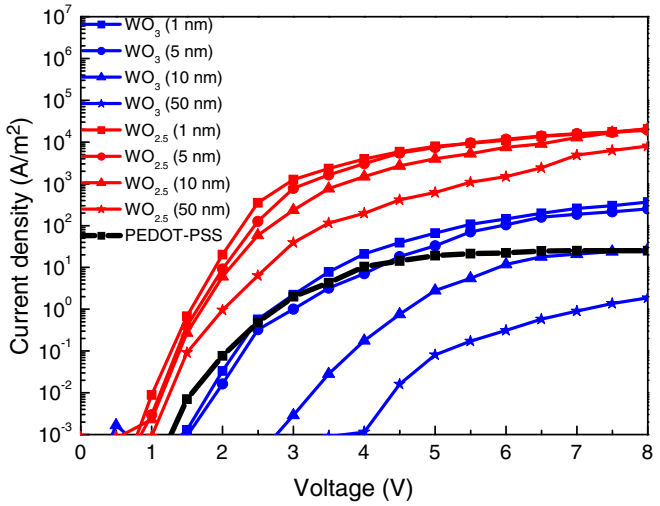

Fig. 4. Current density–voltage (J–V) curves of hole-only devices with the structure ITO/WO_x/F8BT/Au (ITO anode), for x either 3 (stoichiometric tungsten oxide) or 2.5 (tungsten suboxide), for 1, 5, 10 and 50 nm of oxides thicknesses. The J–V curve of a control device using 40 nm PEDOT–PSS for hole injection is also shown.

150 nm thick cathode layer in a dedicated chamber. The cathode was thermally evaporated using a stainless steel shadow mask to define the device area, which was 2.75 mm^2 Au for the HODs and 12.56 mm^2 Al for the OLEDs.

2.5. Device characterization

J–V characteristics were measured with a Keithley 2400 source-measure unit, while luminance and electroluminescence (EL) spectral characteristics were recorded with an Ocean Optics spectrophotometer equipped with fiber optics, assuming a Lambertian emission profile (for the luminance measurements). All the measurements were conducted in ambient conditions.

3. Results and discussion

Fully stoichiometric (WO_3) and substoichiometric with controlled and reproducible stoichiometry ($WO_{2.5}$) tungsten oxide films were deposited as described in Section 2 and Ref. [40]. Prior to device fabrication and characterization, investigation on tungsten oxide films optical, morphological and electrical properties was carried out. Both tungsten oxide layers are transparent in the visible spectrum (where they exhibit transmittance values larger than 90%), as it can be concluded from the transmittance spectra of 10 nm thick films, shown in Fig. 1a, and thus, they are appropriate to be used at the anode side of the device, where usually light extraction occurs. Furthermore, ellipsometry measurements have shown that the dispersion of their refractive indices with regard to the wavelength

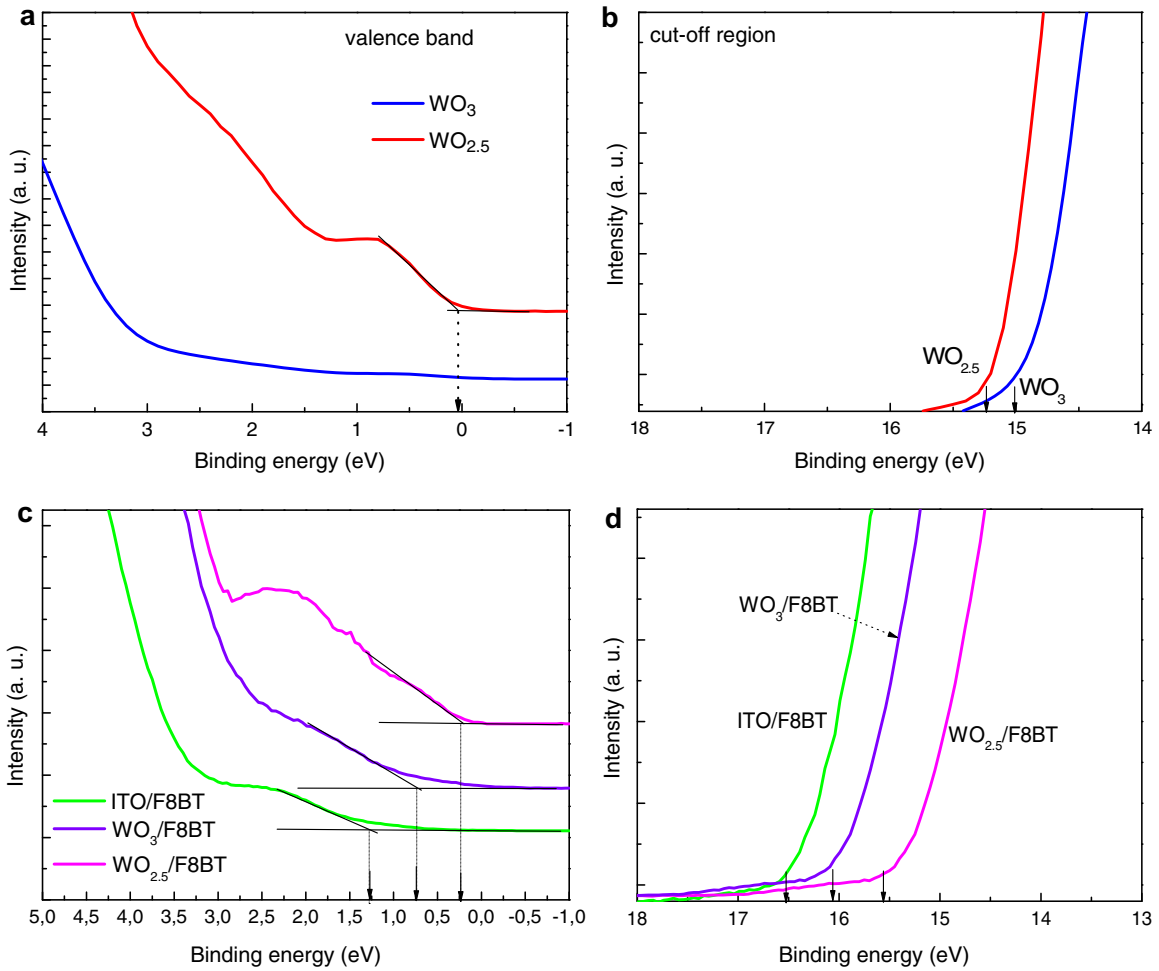

Fig. 5. (a) Valence band and near E_F and (b) cut-off region of UPS spectra of WO_3 and $WO_{2.5}$ 10 nm thick films on ITO substrate, (c) valence band (HOMO region) and (d) cut-off region of UPS spectra of F8BT/WO_3 and F8BT/$WO_{2.5}$ interfaces and of an 1.5 nm F8BT layer.

was dependent on their thickness. For stoichiometric WO_3 films thicker than 10 nm the refractive indices were even lower than that of fused silica (1.45) as seen in Fig. 1b. On the other hand, hydrogen reduced (substoichiometric) $WO_{2.5}$ films exhibit increased refractive indices (as well as extinction coefficients, not shown) compared to WO_3, as also seen in Fig. 1b. Their refractive indices were decreased upon thickness increase and they were saturated at about 2.0 (at $\lambda \sim 540$ nm) for films thicker than 10 nm.

The morphology of these films is of great interest since the film forming properties of an anode interfacial layer deposited on top of the relatively rough surface of ITO (which, as already mentioned above, was not submitted to UV or O_2 plasma treatment) are crucial for the device performance. As it can be seen from SEM images in Fig. 2, the surfaces of both films were quite similar showing a nanostructured morphology. The main difference was in the grain size, which seemed to substantially decrease when films became substoichiometric. WO_3 samples showed a granular surface with grains of about 100 nm (in diameter), composed of smaller ones of 5–10 nm, while for $WO_{2.5}$ films the grain size became less than half. Additionally, the porosity of the tungsten suboxide $WO_{2.5}$ films was also decreased compared to that of WO_3, resulting in better film forming properties (smoother layers and decreased surface roughness) which is beneficial for device performance.

The metallic character of tungsten suboxide films was investigated by measuring their electrical resistivity at various temperatures (above room temperature). From Fig. 3 a resistivity of about 10 Ω cm can be deduced for a 5 nm tungsten suboxide film, which is more than one order of magnitude smaller than the corresponding of its parent stoichiometric of the same thickness (about 120 Ω cm). Moreover, for $WO_{2.5}$, resistivity increased with temperature, while for WO_3 the opposite trend was observed. The above results are clear evidence of the metallic character of the tungsten suboxide, $WO_{2.5}$, in contrast to the WO_3, which exhibits insulating behavior.

Hole-only devices (HODs) were fabricated in order to investigate the hole injection properties of both tungsten oxides. The device structure was ITO/tungsten oxide (1, 5, 10 and 50 nm)/F8BT (70 nm)/Au (Au cathode). Due to the high energy barrier between the work function of Au top

(cathode) electrode (5.2 eV) and the LUMO of F8BT (3.3 eV) [43], no electrons can be injected and flow in these devices and thus, any observed current is exclusively attributed to holes injected from the ITO anode. From the *J–V* characteristics shown in Fig. 4, it is evident that the hole current turn-on voltage for the devices employing $WO_{2.5}$ as HIL is almost half and the current density is up to two orders of magnitude higher than that of the devices with WO_3 as HIL. Furthermore, it is quite impressive that the device characteristics remain almost unaffected, when the oxide thickness is increased from 1 to 10 nm and the device still operates efficiently even for a $WO_{2.5}$ HIL with a thickness of 50 nm. On the contrary, a similar increase of WO_3 thickness results in extremely poor device performance (the devices employing 50 nm of WO_3 show very low currents), due to the insulating character and poor hole injection properties of the stoichiometric oxide. In Fig. 4 the *J–V* characteristic of PEDOT–PSS based control device is also shown for comparison. Strong injection-limited current behavior was observed for this device attributed to poor hole injection properties of the PEDOT–PSS modified anode contacts.

In order to shed light to the increased hole injection efficiency of substoichiometric tungsten oxide relative to its parent oxidized one, the electronic structure of thin films and interfaces with F8BT was explored using UPS. Valence band spectra of both oxides are shown in Fig. 5a. The WO_3 valence band consists mainly of occupied O 2*p* orbitals and its maximum (VBM) is located about 3 eV below the Fermi level. In contrast to stoichiometric WO_3, the valence band spectrum of the substoichiometric oxide $WO_{2.5}$ shows a large density of occupied sub-bandgap states centered at 0.7 and 2.2 eV below the Fermi level that are attributed mainly to W 5*d* and with a minor contribution of O 2*p* states. Note that the peak centered at 0.7 eV extends almost up to the Fermi level (VB edge near 0 eV for the $WO_{2.5}$), implying the reduced suboxide has no bandgap. In this manner, conversion from the wide-bandgap, insulating WO_3 to almost zero bandgap nearly metallic $WO_{2.5}$, through the excellent control of their stoichiometry due to the hydrogen reduction, is achieved.

The work functions of both tungsten oxides (WO_3 and $WO_{2.5}$, respectively) were also determined from the photoemission secondary-electron cut-off and shown in Fig. 5b. They are very high, with the corresponding values of 6.2 eV for the stoichiometric, in accordance with previously published results [25], and about 5.9 eV for the substoichiometric one. The work function of ITO was also measured and it was found to be ~4.4 eV (not shown). Note that ITO substrates were not subject to any surface activation by oxygen plasma treatment in order to investigate the intrinsic hole injection properties of tungsten oxide layers despite the large hole injection barrier rising from the low work function of these ITO substrates. The large work function values for both tungsten oxides indicate the formation of large positive interfacial dipoles (negative pole pointing towards the oxide and positive towards ITO) of about 1.8 eV at the ITO/WO_3 interface and of a slightly smaller, of about 1.5 eV, at the ITO/$WO_{2.5}$ interface, thus, leading to the increased work function of the ITO/WO_x modified interface. As a result, the hole injection barrier at the interface with the F8BT polymer is expected to be reduced compared to the ITO/F8BT interface. The energy distance between the E_F and the HOMO edge of a thin F8BT layer on each substrate reflects the hole injection barrier. The energy level alignment of F8BT on each substrate was determined from the valence band spectra of a thin F8BT layer (approximately 1.5 nm) spin-coated on top of the substrate. The corresponding UPS results are shown in Fig. 5c. First, the HOMO level of the F8BT layer was measured and found about 1.25 eV below the ITO Fermi level, resulting in a large hole injection barrier. On the other hand, the position of the F8BT HOMO is different at the interface with each oxide. The HOMO edge of F8BT on WO_3 moves closer to the Fermi level, lying about 0.75 eV lower than E_F, while the HOMO edge of F8BT on $WO_{2.5}$ is lying about 0.25 eV below Fermi level, thus, leading to a large reduction of the hole injection barrier. Moreover, the work function of F8BT on both oxide substrates was determined from the UPS cut-off region (Fig. 5d). The work function of a F8BT layer directly spin coated on top of an ITO substrate was estimated about 4.65 eV. In the case of thin F8BT layers deposited on both tungsten oxides the effective work functions (W_F) were increased to 5.15 and 5.65 eV for deposition on top of WO_3 and $WO_{2.5}$, respectively. This indicates the formation of negative interfacial dipoles for both WO_x/F8BT interfaces, a large one of about 1.25 eV at WO_3/F8BT interface and of a significantly smaller of about 0.25 eV at $WO_{2.5}$/F8BT interface. These results show that work function alone does not correctly predict the interfacial energy alignment due to the different direction interfacial dipoles that exist at the corresponding ITO/WO_x/F8BT interfaces.

The corresponding energy level diagram showing the energy level alignment on the ITO/WO_x and WO_x/F8BT interfaces, as determined from the UPS measurements discussed above, is presented in Fig. 6b. The OLED device architecture employing the tungsten oxides as HILs and the chemical structure of F8BT are shown in Fig. 6a. The conduction band (CB) edge of WO_3 was extracted by subtracting the optical bandgap energy (3.15 eV as it was previously calculated [40]) from the valence band edge (thus, the CB edge is about 0.15 eV above the Fermi level, indicating a strong n-type character). In the case of ITO/WO_3/F8BT interfaces large barriers for either hole injection from ITO to the valence band of WO_3 (about 3.0 eV below Fermi level) or for electron extraction from the HOMO of F8BT through the CB of WO_3 (energy difference of about 0.9 eV) are observed (Fig. 6b, left). On the contrary, for $WO_{2.5}$ these barriers are nearly eliminated due to the formation of the sub-bandgap electronic states (Fig. 6b, right), which enable the injection of charge through a suggested mechanism, including two individual processes: (1) barrierless hole injection via the occupied gap states and (2) charge generation process at the $WO_{2.5}$/F8BT interface and electron extraction via the upper gap states and/or the CB. The proposed charge injection mechanism is also illustrated in Fig. 6b.

Next, bipolar devices using F8BT as emissive layer, with the simple structure ITO/tungsten oxide (5 nm)/F8BT (70 nm)/Al were studied for LED characterization. The choice of the optimum oxide thickness was based on con-

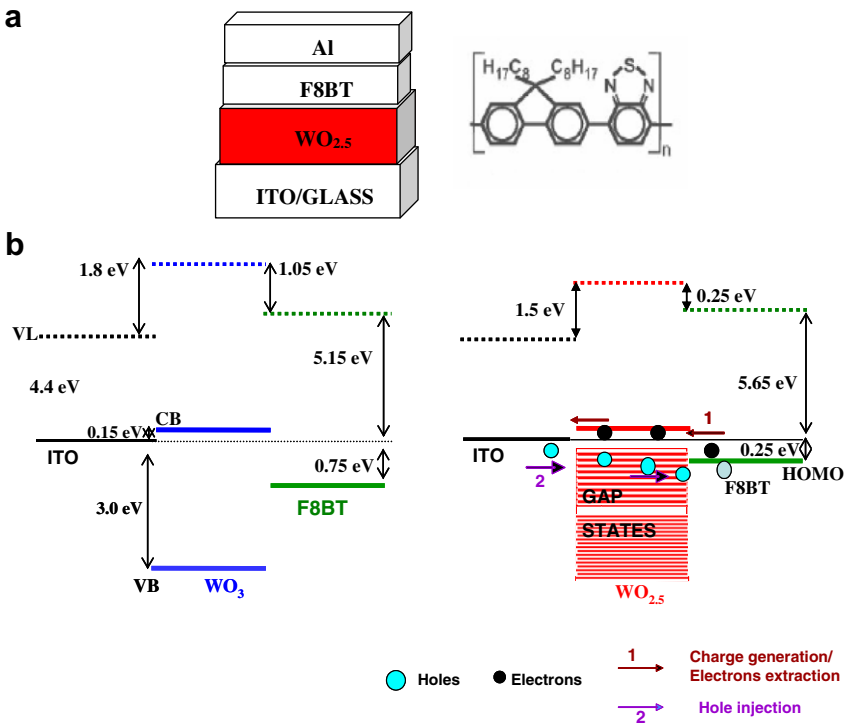

Fig. 6. (a) F8BT based OLED architecture employed tungsten oxides as anode interfacial layers (left) and the chemical structure of F8BT (right). (b) The corresponding energy level diagram and illustration of the proposed hole injection mechanism for ITO/WO_3/F8BT (left) and ITO/WO_x/F8BT (right) interfaces.

ductivity results as well as on microcavity efficiency simulations and found about 5 nm (devices with tungsten oxide layers thinner than 1 nm exhibited increased leakage currents, especially in the case of the stoichiometric one). The external EL quantum efficiency of the proposed devices is expected to be influenced by the corresponding light outcoupling efficiency, caused by microcavity effects that are present on a multilayer dielectric structure. Each layer thickness, along with its respective spectral dependent complex refractive index, affects the outcoupling efficiency and has to be calculated for an optimum device efficacy. Herein, the adopted electromagnetic model considers each emission point inside the active layer as a randomly oriented hertz dipole. For the simulation of the interference phenomena inside the multilayer structure and the outcoupling total radiation power or the radiation intensity at any viewing angle, the transmission line calculation schemes have been applied [44]. Furthermore, a critical parameter that also influences the microcavity efficiency is the location of the emission point which is usually located very close to the p–n junction interface. Using the aforementioned calculation scheme, the outcoupling OLED efficiency has been examined by testing both types of tungsten oxides (stoichiometric WO_3 and reduced, $WO_{2.5}$) as a hole injection-transport layer. From Fig. 7 we remark that for the wavelength of 540 nm (peak emission of F8BT), the insertion of reduced tungsten oxide results in higher outcoupling efficiency compared to WO_3, at both oxide thicknesses tested, due to better matching of its refractive index with that of ITO and F8BT [44]. Better results were obtained for $WO_{2.5}$ films with a thickness of 10 nm and more, which exhibit refractive index with a value of 1.9 (instead of the optimum 1.6 for an ultra thin ~1 nm thick WO_3 film) and thus, match perfectly that of F8BT (about 1.9 also).

Experimental *J–V–L* curves are shown in Fig. 8a and Table 1. In WO_3-based devices, delayed and relatively poor light emission is observed. On the contrary, in tungsten suboxides-based devices more than one order of magnitude higher luminances and currents are observed, accompanied by a significant decrease in the turn-on voltage. It is worthwhile to mention that the maximum current density of 7000 A/m^2 and the maximum luminance of 12,000 cd/m^2 are among the best values reported for F8BT based devices with Al cathode, when no additional electron injection/hole blocking layer is incorporated in the device.

It should also be mentioned that there is a small offset between current and light turn-on, as it can be seen in Fig. 8a. The reason for the slightly delayed light emission stems from the large electron injection barrier at the Al/F8BT interface (since the LUMO of F8BT is located at about 3.3 eV the barrier for electron injection from aluminum with a W_F of 4.2 eV is almost 1.0 eV, as it can be seen in Fig. 6b), while the hole injecting tungsten suboxide/F8BT interface is highly efficient. This results in an unbalanced charge injection and thus, build-up of holes at the F8BT/Al interface when an external bias is applied. The electric field is then redistributed, dropping primarily over the Al/F8BT interface, enhancing the electron injection (hole assisted electron injection mechanism) [7]. Nevertheless,

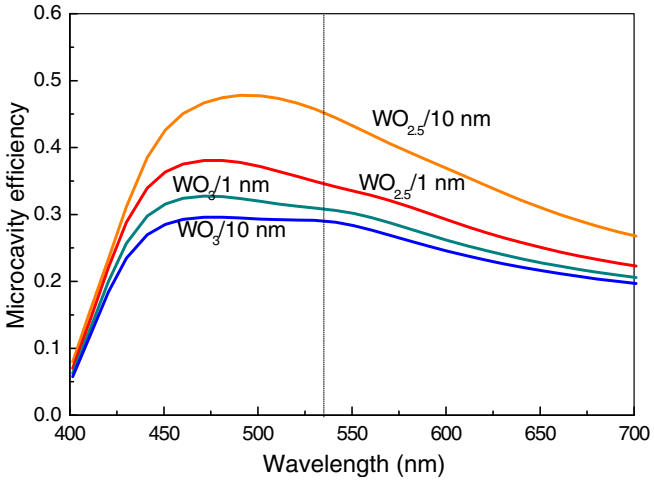

Fig. 7. Normalized outcoupling efficiency due to microcavity effect for stoichiometric (WO_3) and reduced ($WO_{2.5}$) tungsten oxides with different thicknesses.

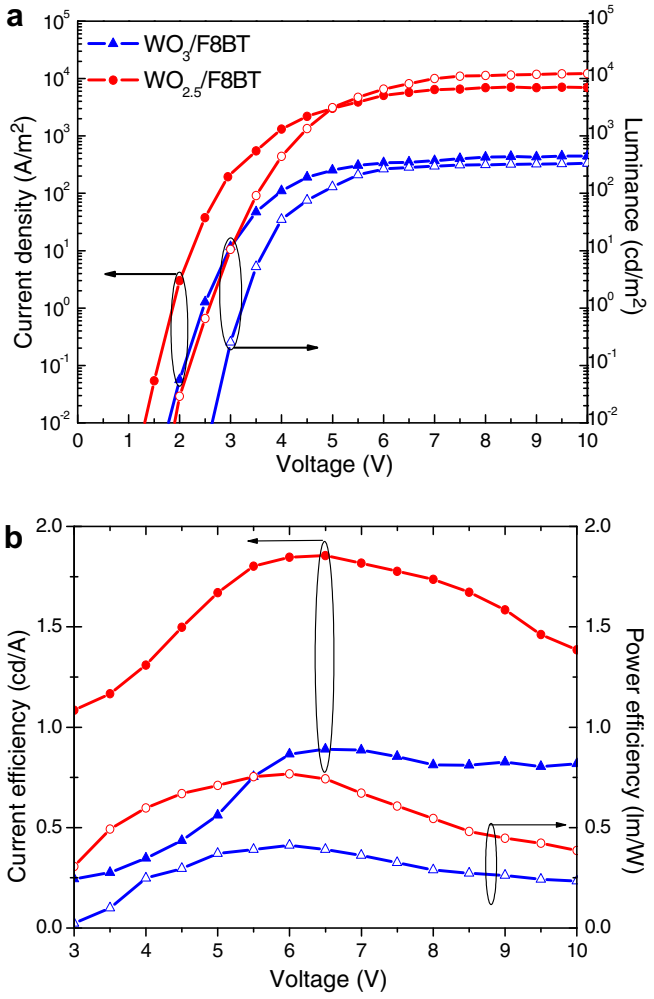

Fig. 8. (a) Current density (solid symbols)–luminance (open symbols)–voltage characteristics and (b) current efficiency (solid symbols)–power efficiency (open symbols) of OLEDs with 5 nm thick WO_3 (triangles) and $WO_{2.5}$ (cycles) as hole injection layers in F8BT based OLEDs.

Table 1
Performance parameters of F8BT-based devices taken from the characteristic curves of Figs 8 and 9 (Data reported in the third row, concerning devices with WO_3 as HIL and $WO_{2.5}$ as EIL, are taken from Ref. [34]).

HIL	EIL	$V_{turn\text{-}on}$ (V) (at 10 cd/m^2)	J_{max} (A/m^2)	L_{max} (cd/m^2) [at 8 V]	Max luminous efficiency (cd/A)	Max power efficiency (lm/W)
WO_3	_	3.5	500	400	0.8	0.4
$WO_{2.5}$	–	3.0	7000	11,800	1.9	0.9
WO_3	$WO_{2.5}$	3.5	3200	11,000	4.5	3.0
$WO_{2.5}$	$WO_{2.5}$	2.5	4000	25,000	7.0	4.5

the device efficiencies are not optimized yet. The current efficiency and power efficiency curves are shown in Fig. 8b. Current and power efficiency values of about 1.9 cd/A and 0.9 lm/W at 5.5 V for the $WO_{2.5}$-based device are more than 100% improved compared to the WO_3-based device, but still low compared to the state of the art devices [10] due to a number of possible loss mechanisms. Since charge injection is still unbalanced a shift of the recombination zone towards the poor injecting contact takes place. As a consequence, some of the generated photons can be quenched at the Al/F8BT interface. Moreover, the high charge density at the same interface (accumulation of holes) can lead to a leakage current with a consequent increase of the current density not accompanied by an increase in the luminance. These phenomena limit the device efficiency despite the superior hole injection characteristics of $WO_{2.5}$.

In order to enhance device efficiency, it is imperative to lower the barrier for electron injection through insertion of an efficient EIL. In our recent publication, we used thin $WO_{2.5}$ layers to enhance electron injection from an Al cathode in F8BT-based devices. Herein, we have presented clear evidence for the highly efficient hole injection and transport properties of the same tungsten suboxide ($WO_{2.5}$). Based on the superior optical and electronic characteristics of this metallic oxide (occupied sub-bandgap

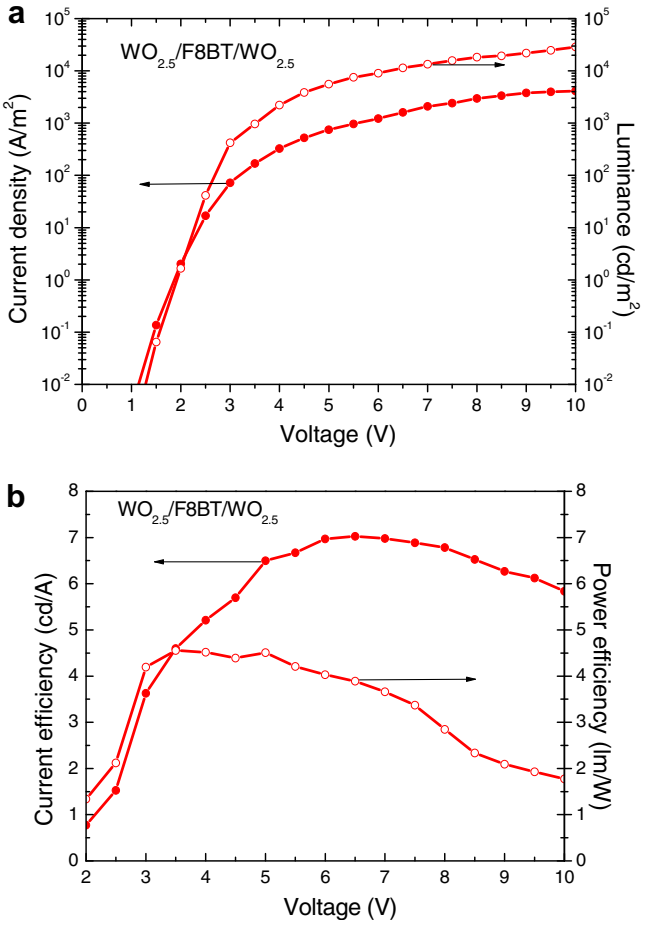

Fig. 9. (a) Current density (solid cycles)–luminance (open cycles)–voltage characteristics and (b) current efficiency (solid cycles)–power efficiency (open cycles) of symmetric F8BT based OLEDs with $WO_{2.5}$ as both hole and electron injection layers in F8BT based OLEDs.

states, increased conductivity, optimum optical and morphological properties), we demonstrate highly efficient symmetric OLEDs based on F8BT using $WO_{2.5}$ as both anode and cathode interfacial layers. In Fig. 9a *J–V–L* curves for devices where the hole injection occurs through a 5 nm thick $WO_{2.5}$ layer, while another $WO_{2.5}$ layer, about 1 nm thin, deposited on top of F8BT serves as electron injection layer, are shown. According to Fig. 6b excellent energy level alignment between the CB of $WO_{2.5}$ (presence of sub bandgap states near the E_c) and the Al cathode is achieved, thus, permitting the formation of highly efficient electron injecting contact, as has been previously demonstrated [40]. Besides, the increased electron conductivity (n-type material) of tungsten suboxide results in enhanced electron transport through its upper occupied sub-bandgap states and/or its CB to the LUMO of F8BT. Luminances up to 25,000 cd/m^2 and efficiencies up to 7.0 cd/A and 4.5 lm/W were obtained. These values are 75% and 50%, respectively, higher than those reported before from our group for devices using WO_3 as HIL and $WO_{2.5}$ as EIL [35] (those results are also included in Table 1) and among the best efficiencies reported so far for EL devices incorporating thin F8BT layers. This improvement is attributed mainly to the highly efficient hole injection and transport properties of $WO_{2.5}$ used as anode interfacial layer instead of WO_3.

The stability of unencapsulated EL devices with substoichiometric $WO_{2.5}$ as efficient HIL upon storage in air was also tested. The luminance and driving voltage versus time for F8BT-based OLEDs incorporating a 5 nm thin $WO_{2.5}$ HIL and Al cathode, operated in ambient conditions and biased at a constant current density of ~200 A/m^2 is shown in Fig. 10. The initial luminance values were $L = 580$ cd/m^2 at operational voltage 3.5 V. After 700 h luminance decreases to $L = 490$ cd/m^2 corresponding to only 17% decrease for both devices. Similarly, in devices with 5 nm $WO_{2.5}$ layer at the anode side and 1 nm $WO_{2.5}$ layer at the F8BT/cathode interface, the luminance was reduced from 2500 cd/m^2 to 2100 cd/m^2 (corresponding to 15% decrease) over the 700 h testing period, biased at constant current density of ~200 A/m^2. The impressive stability of our $WO_{2.5}$ incorporating OLEDs represents a very significant advantage, since conventional PLEDs based on PEDOT–PSS show reduced stability due to hydroscopic and acidic nature of PSS.

We should note here that it is, to the best of our knowledge, the first time ever been reported that, the exact same material can be used to enhance both hole and electron injection/transport in an OLED device. We propose that, due to their occupied sub-bandgap states located near the Fermi level, their metallic-like conductivity and optimized surface morphology, tungsten and, also, molybdenum substoichiometric oxides (as our recent studies have also revealed and we will publish elsewhere) obtained through controlled hydrogen reduction exhibit unique charge injection/transport properties compared to their parent stoichiometric ones. Similar results were recently demonstrated by our group [45] for reduced molybdenum oxide consisting of Mo^{+6} and Mo^{+5} oxidation states and by other groups, obtained after annealing of MoO_3 [33]. The unique benefits from the use of these materials as a charge injection/transport layers in OLEDs and, in general, in organic optoelectronics are clearly justified by the above and our previous study [39], paving, thus, the way for low-cost and simple fabrication of organic electronics using multi functional materials with tunable properties and multiple applications.

4. Summary and conclusions

In conclusion, we have demonstrated that the tungsten substoichiometric oxide with precise stoichiometry, $WO_{2.5}$,

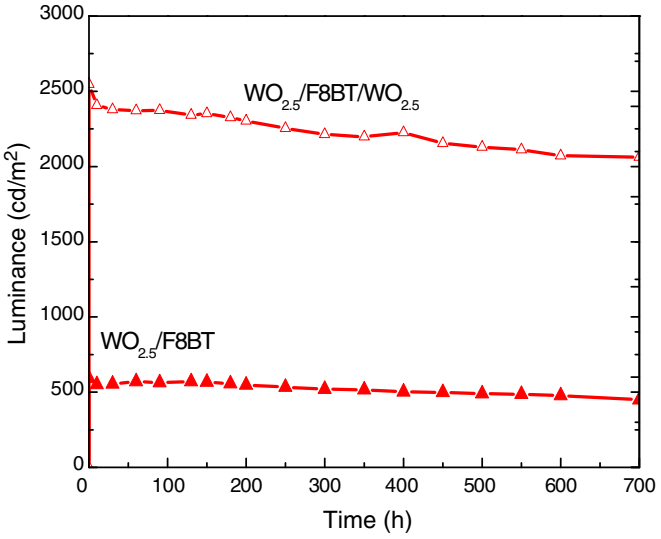

Fig. 10. Stability data for unencapsulated OLEDs based on tungsten suboxide $WO_{2.5}$ as HIL: Luminance and operational voltage versus time of operation in air at room temperature with a constant driving current density of 200 A/m^2.

synthesized by the controlled hydrogen reduction of WO_3, exhibits unique hole injection properties, due to its sub-bandgap occupied states that are positioned between the anode Fermi level and the oxide valence band edge and, therefore, greatly facilitate hole injection. Furthermore, this oxide exhibits metallic properties and smooth surface morphology, contributing to improved conductivity and substrate coverage in comparison with its parent stoichiometric tungsten trioxide. An almost zero hole injection barrier and also highly efficient hole injection properties were achieved for F8BT-based hole-only and OLED devices, incorporating $WO_{2.5}$ as anode interfacial layer. Electroluminescent devices using $WO_{2.5}$ as both, hole and electron injection/transport layer, showed remarkably high efficiencies up to 7 cd/A and 4.5 lm/W, while stability studies revealed that unencapsulated OLEDs incorporating substoichiometric tungsten oxides are exceptionally stable. According to our results substoichiometric metal oxides obtained through controlled hydrogen reduction exhibit increased charge injection properties and outperform their parent stoichiometric ones, thus, representing a novel class of functional materials with tunable properties appropriate for use in low-cost organic optoelectronic devices.

References

[1] S.R. Forrest, Nature 428 (2004) 911.
[2] C. W Tang, S.A. Van Slyke, Appl. Phys. Lett. 51 (1987) 913.
[3] J.H. Burroughes, D.D.C. Bradley, A.R. Brown, R.N. Marks, K. Mackay, R.H. Friend, P.L. Burns, A.B. Holmes, Nature 347 (1990) 539.
[4] R.H. Friend, R.W. Gymer, A.B. Holmes, J.H. Burroughes, R.N. Marks, C. Taliani, D.D.C. Bradley, D.A. Dos Santos, J.L. Brédas, M. Lögdlund, W.R. Salaneck, Nature 397 (1999) 121.
[5] H. Ma, H.-L. Yip, F. Huang, A.K.-Y. Jen, Adv. Funct. Mater. 20 (2010) 1371.
[6] L.C. Palilis, M. Vasilopoulou, D.G. Georgiadou, P. Argitis, Org. Electron. 11 (2010) 887.
[7] M. Sessolo, H.J. Bolink, Adv. Mater. 23 (2011) 1829.
[8] T. Matsushima, Y. Kinoshita, H. Murata, Appl. Phys. Lett. 91 (2007) 253504.
[9] H. You, Y. Dai, Z. Zhang, D. Ma, J. Appl. Phys. 101 (2007) 026105.
[10] D. Kabra, L.P. Lu, M.H. Song, H.J. Snaith, R.H. Friend, Adv. Mater. 22 (2010) 3194.
[11] H. J Bolink, E. Coronado, J. Orozco, M. Sessolo, Adv. Mater. 21 (2009) 79.
[12] S.A. Haque, S. Koops, N. Tokmoldin, J.R. Durrant, J.S. Huang, D.D.C. Brandley, E. Palomares, Adv. Mater. 19 (2007) 683.
[13] N. Tokmoldin, N. Griffiths, D.D.C. Bradley, S.A. Haque, Adv. Mater. 21 (2007) 3475.
[14] H.J. Bolink, E. Coronado, D. Repetto, M. Sessolo, E.M. Barea, J. Bisquert, G. Garcia-Belmonte, J. Prochazka, L. Kavan, Adv. Funct. Mater. 18 (2008) 145.
[15] J. Meyer, S. Hamwi, T. Bülow, H.-H. Johannes, T. Riedl, W. Kowalsky, Appl. Phys. Lett. 91 (2007) 113506.
[16] J. Meyer, T. Winkler, S. Hamwi, S. Schmale, H.-H. Johannes, T. Weinmann, P. Hinze, W. Kowlasky, T. Riedl, Adv. Mater. 20 (2008) 3839.
[17] M. Kröger, S. Hamwi, J. Meyer, T. Riedl, W. Kowalsky, A. Kahn, Org. Electron. 10 (2009) 932.
[18] S. Hamwi, J. Meyer, M. Kröger, T. Winkler, M. Witte, T. Riedl, A. Kahn, W. Kowalsky, Adv. Funct. Mater. 20 (2010) 1.
[19] C.C. Chang, M.T. Hsieh, J.F. Chen, S.W. Hwang, C.H. Chen, Appl. Phys. Lett. 89 (2006) 253504.
[20] J. Meyer, S. Hamwi, S. Schmale, T. Winkler, H.-H. Johannes, T. Riedl, W. Kowalsky, J. Mater. Chem. 19 (2009) 702.
[21] Y.H. Kim, S. Kwon, J.H. Lee, S.M. Park, Y.M. Lee, J.W. Kim, J. Phys. Chem C 115 (2011) 6599.
[22] F. Wang, X. Qiao, T. Xiong, D. Ma, Appl. Phys. Lett. 105 (2009) 084518.
[23] M.J. Son, S. Kim, S. Kwon, J.W. Kim, Org. Electron. 10 (2009) 637.
[24] H. Kanno, R.J. Holmes, Y. Sun, S.K. Cohen, S.R. Forrest, Adv. Mater. 18 (2006) 339.
[25] M. Kröger, S. Hamwi, J. Meyer, T. Riedl, W. Kowalsky, A. Kahn, Appl. Phys. Lett. 95 (2009) 12301.
[26] S. Hamwi, J. Meyer, M. Kröger, T. Winkler, M. Witte, T. Riedl, A. Kahn, W. Kowalsky, Adv. Funct. Mater. 20 (2010) 1762.
[27] Y. Sun, C.J. Takacs, S.R. Cowan, J.H. Seo, X. Gong, A. Roy, A. Heeger, Adv. Mater. 23 (2011) 226.
[28] Y. Sun, G.C. Welch, W.L. Leong, C.J. Takacs, G.C. Bazan, A.J. Heeger, Nat. Mater. 11 (2012) 44.
[29] J. Gao, G.L. Perkins, J.M. Luther, M.C. Hanna, H-Y Chen, O.E. Semonin, A.J. Nozik, R.J. Ellingson, M.C. Beard, Nanoletters 11 (2011) 3263.
[30] S.Y. Chiam, B. Dasgupta, D. Soler, M.Y. Leung, H. Liu, Z.E. Ooi, L.M. Wong, C.Y. Jiang, K.L. Chang, J. Zhang, Sol. Energ. Mat. Sol. C. 99 (2012) 197.
[31] E.L. Ratcliff, J. Meyer, K.X. Streirer, A. Garcia, J.J. Berry, D.S. Ginley, D.C. Olson, A. Kahn, N.R. Armstrong, Chem. Mater. 23 (2011) 4988.
[32] M.T. Greiner, M.G. Helander, Z.B. Wang, W.M. Tang, J. Qiu, Z.H. Lu, Appl. Phys. Lett. 96 (2010) 213302.
[33] A. Buckley, D. Pickup, C. Yates, Y. Zhao, D. Lidzey, J. Appl. Phys. 109 (2011) 084509.
[34] Irfan, H. Ding, F. So, Y. Gao, J. Photonics. Energy 1 (2011) 011105-1.
[35] A. Rothschild, J. Sloan, R. Tenne, J. Am. Chem. Soc. 122 (2000) 5169–5179.
[36] Z.S. Houweling, J.W. Geus, M. de Jong, P-P.R.M.L. Harks, K.H.M. van der Werf, R.E.I. Schropp, Mater. Chem. Phys. 131 (2011) 357.
[37] J. Meyer, K. Zilberberg, T. Riedl, A. Kahn, J. Appl. Phys. 110 (2011) 033710.
[38] M. Merz, J. Eisenmenger, B. Heinz, P. Ziemann, Phys. Rev. B 66 (2002) 184102.
[39] M. Vasilopoulou, L.C. Palilis, D.G. Georgiadou, P. Argitis, S. Kennou, L. Syggelou, I. Kostis, G. Papadimitropoulos, N. Konofaos, A. Iliadis, D. Davazoglou, Appl. Phys. Lett. 98 (2011) 123301.
[40] M. Vasilopoulou, L.C. Palilis, D.G.Georgiadou, A.M. Douvas, P. Argitis, S. Kennou, L. Syggelou, G. Papadimitropoulos, I. Kostis, N.A. Stathopoulos, D. Davazoglou, Adv. Funct. Mater. 21 (2011) 1489.
[41] G. Papadimitropoulos, N. Vourdas, K. Giannakopoulos, M. Vasilopoulou, D. Davazoglou, J. Appl. Phys. 109 (10) (2011) 103527.
[42] N. Vourdas, G. Papadimitropoulos, I. Kostis, M. Vasilopoulou, D. Davazoglou, Thin Solid Films 519 (2011) 5748.
[43] Y. Nakayama, K. Morii, Y. Suzuki, H. Machida, S. Kera, N. Ueno, H. Kitagawa, Y. Noguchi, H. Ishii, Adv. Funct. Mater. 19 (2009) 3746.
[44] N.A. Stathopoulos, M. Vasilopoulou, L.C. Palilis, D.G. Georgiadou, P. Argitis, Appl. Phys. Lett. 93 (2008) 083310.
[45] M. Vasilopoulou, L.C. Palilis, D.G. Georgiadou, S. Kennou, I. Kostis, D. Davazoglou, P. Argitis, Appl. Phys. Lett. 100 (2012) 013311.